Title

Fatigue crack growth rates of X100 steel welds in high pressure hydrogen gas considering residual stress effects

Authors

Ronevich, Joseph A
D'Elia, Christopher R
Hill, Michael R

Publication Date

2018-05-01

DOI

10.1016/j.engfracmech.2018.02.030

Peer reviewed

Fatigue crack growth rates of X100 steel welds in high pressure hydrogen gas considering residual stress effects

Joseph A. Ronevich[1], Christopher R. D'Elia[2], Michael R. Hill[2]

[1]Sandia National Laboratories, Livermore, CA, USA

[2]Department of Mechanical and Aerospace Engineering, University of California Davis, Davis, CA, USA.

Abstract:

Fatigue crack growth rate (FCGR) data were measured in high pressure hydrogen gas versus stress intensity factor range (ΔK) in specimens removed from a X100 welded steel pipe. Three distinct regions of the pipe weld were examined: base metal, weld fusion zone, and heat affected zone. Tests were performed at a load ratio (R) of 0.5, frequency of 1 Hz, and at a hydrogen gas pressure of 21 MPa. Tests were also performed in air at 10 Hz as a reference. Fatigue crack growth rates were observed to be over an order of magnitude higher for tests performed in hydrogen compared to the rates from tests in air. Residual stress measurements were collected on identical specimens cut from the base metal, weld, and heat affected zone to account for their influence on measured FCGR data. The slitting method provided residual stress and residual stress intensity factor (K_{res}), the effect of which was removed from the FCGR data using K_{norm} in order to provide a more direct comparison of crack growth resistance of the base metal, weld and heat affected zone. Prior to accounting for residual stress, FCGR in hydrogen gas appeared to be highest in the weld fusion zone. After accounting for residual stress effects, the weld fusion zone FCGR data converged to the base metal FCGR data, which underscores the importance of accounting for residual stress effects when assessing fatigue performance.

Keywords: Hydrogen embrittlement, residual stress, high strength pipeline steels, fatigue crack growth rate, high pressure hydrogen

1. Introduction:

Steel transmission pipelines have provided a safe and reliable system for transporting hydrogen gas for many decades. This has been demonstrated through the thousands of kilometers of hydrogen pipe operated in the United States and Europe [1]. However, the network of hydrogen pipes is typically operated at relatively modest and constant pressures, e.g. below 14 MPa. As the demand for hydrogen increases, the operating pressure of the pipelines is anticipated to expand beyond the current operating envelope and fluctuations of pressure may be incurred on the pipes. While the current infrastructure of hydrogen pipelines is a testament to their reliability, the prospect of changed operating conditions needs to be considered judiciously. Pipeline operation at higher pressures with variations in demand has the potential to generate fatigue loading through pressure cycling. Pressure cycling can promote a failure mode that is otherwise non-existent when the pipe is operated under static conditions, i.e. hydrogen accelerated fatigue crack growth. In this embrittlement phenomenon, fatigue cracks can grow more than 40 times faster in a hydrogen environment compared to their growth in air [2-5].

Higher strength hydrogen steel pipelines are an attractive pathway to reduce costs as outlined in a recent paper [6]. The natural gas industry employs thin-walled, high-strength pipes for cost savings. However, for hydrogen pipelines and applicable pipeline code, ASME B31.12, thickness limits are currently placed on higher strength pipes. The added thickness premium nullifies the cost savings that would be gained if similar codes such as the natural gas code ASME B31.8 were permitted. Part of the

conservatism of design codes for hydrogen pipelines is a lack of experimental work on fatigue behavior of higher strength pipelines in a hydrogen environment. Welds, in particular are an added area of concern. It is well-known that the welding process can introduce defects as well as residual stress fields. At present, only a few studies have explored fatigue behavior of pipeline steel welds in hydrogen [2,5].

Residual stresses can influence fatigue behavior depending on their magnitude and sign (i.e. positive or negative); furthermore, in higher strength materials, residual stresses can be high, as they scale with yield strength. In this study, the slitting method (formerly called crack compliance) was used to determine residual stress in fatigue crack growth rate test specimens as a function of position along the crack path, and also the residual stress intensity factor as a function of crack size. These data enable a more complete characterization of the fatigue behavior, by decoupling the effects of residual stress to provide an improved understanding of fatigue performance. Ultimately, this knowledge can improve understanding of the fatigue performance of welded high strength pipelines in hydrogen to enable their use in hydrogen infrastructure.

The overall goal of this work is to develop a comparison of fatigue crack growth rate (FCGR) properties of X100 welded pipe, in high pressure hydrogen, at various positions relative to the weld, that is unbiased by weld residual stress. A first objective is to measure FCGR in 21 MPa hydrogen gas of specimens removed from X100 pipeline steel welds at the weld fusion zone (WFZ), the heat affected zone (HAZ), and base metal (BM). A second objective is to measure residual stress and the residual stress intensity factor, K_{res}, in the specimens used for FCGR testing. A third objective is to use values of K_{res} to remove the effects of residual stress and provide a comparison, unbiased by residual stress, of FCGR in the WFZ, HAZ, and BM regions of X100 welded pipe.

2. Methods

2.1 Specimen Preparation

FCGR testing was performed on specimens removed from an API 5L X100 gas metal arc welded pipe. The pipe was an experimental pipe fabricated in the late ‘90s with a nominal wall thickness of 19 mm and a mean diameter of 1.3 m. The yield strength of the X100 pipe was previously measured in the longitudinal (731 MPa) and transverse (910 MPa) directions. Mechanical property values reported represent the average yield strengths that were obtained from multiple measurements performed on round tensile bars with gauge lengths that varied from 25 to 51 mm. The chemical composition of the base metal is shown in Table 1. The supplier of the pipe is kept anonymous as are the details of the welding process. Figure 1a shows the section of the X100 pipe containing a gas metal arc girth weld. The orientation of material in the pipe is identified by the directions longitudinal “L”, circumferential “C”, and radial “R”. The weld was revealed through macroetching with 2% Nital solution and is shown in Fig. 1b. The distinct features of the weld were visible: WFZ, HAZ, BM, and multiple weld passes. The microstructures of the BM and WFZ are shown in Fig. 2. Figure 2a shows the BM microstructure which consisted of fine ferrite grains and bainite and Fig. 2b shows that the WFZ consisted of bainite and acicular ferrite.

Table 1: Chemical Composition of X100 Base Metal (wt .pct)

Fe	C	Mn	P	S	B	Si	Cu	Ni	Cr	Mo	Nb	Ti	Al
Bal	0.085	1.69	0.013	<0.001	0.0015	0.26	0.14	0.24	0.19	0.17	0.047	0.017	0.029

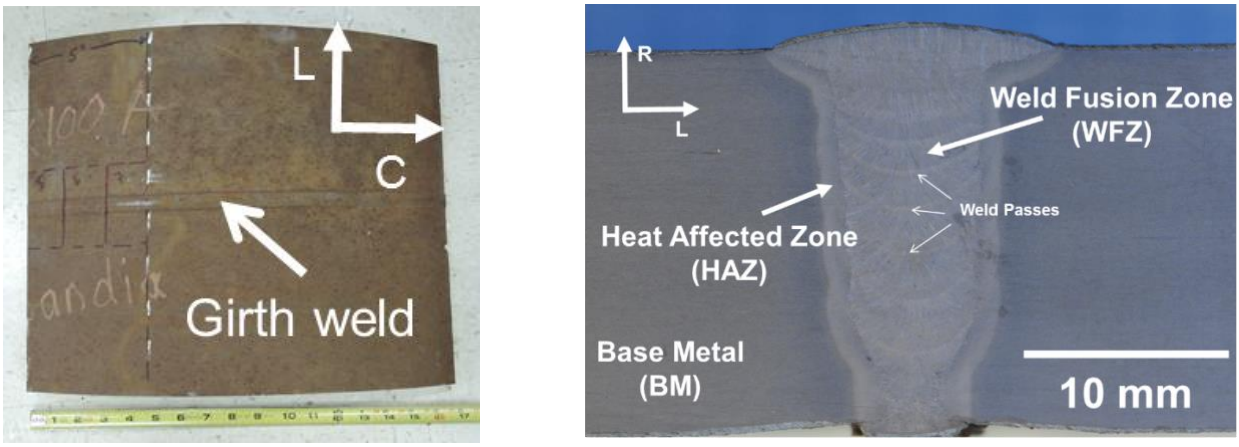

(a) (b)

Figure 1 – (a) Optical image of a section of X100 girth welded pipe, (b) Macroetched image of gas metal arc weld which reveals distinct sections of weld: weld fusion zone (WFZ), heat affected zone (HAZ) and multiple weld passes.

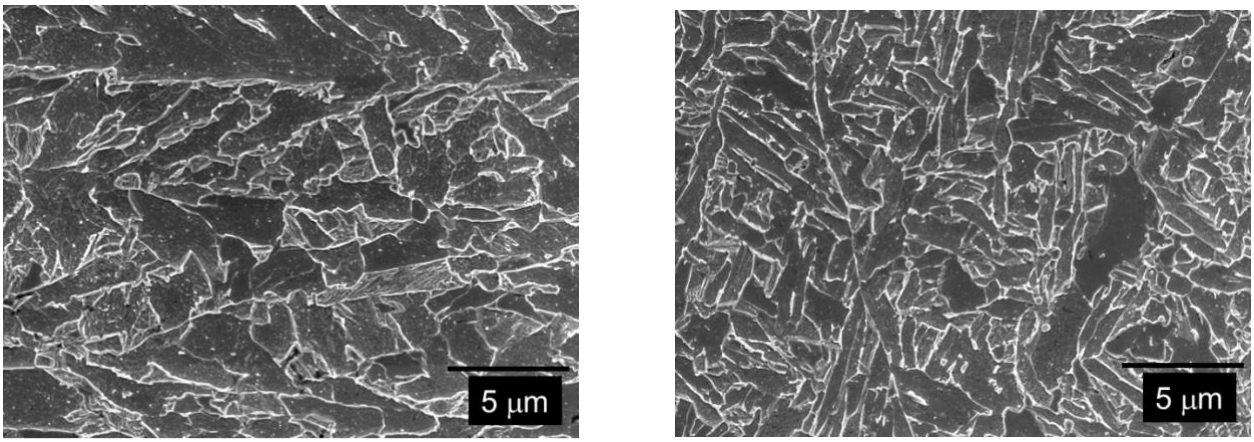

(a) (b)

Figure 2 – Scanning electron microscope images of (a) base metal and (b) weld fusion zone of X100 weld. Images were captured in the longitudinal-radial plane (i.e. same plane as Fig. 1b).

Test specimens were extracted from the welded pipe in order to examine three specific regions: base metal, weld fusion zone, and heat affected zone. Compact tension, C(T), specimens were extracted from the BM in the C-L orientation. The nomenclature C-L means that the load was applied in the circumferential direction and the crack extended in the longitudinal direction. Eccentrically loaded single edge cracked tension, ESE(T), specimens were extracted in the L-R orientation such that the crack plane was located either in the center of WFZ or HAZ and the crack propagated radially. The two different specimen geometries (C(T) and ESE(T)) were used to accommodate the material size constraint of the parent pipe. C(T) specimens were machined with the following dimensions: width (W) = 26.4 mm, thickness (B) = 12.7 mm with side-grooves to final thickness of 11.2 mm, precrack starter notch length-to-width ratio (a/W) = 0.2. The ESE(T) specimens were machined to the following dimensions: width (W) = 12.7 mm, thickness (B) = 3.18 mm, precrack starter notch length-to-width ratio (a/W) = 0.2. Figure

3 shows the approximate location of the ESE(T) specimen removals overlaid on the macroetched weld. The approximate locations are shown for specimens to test the WFZ and HAZ.

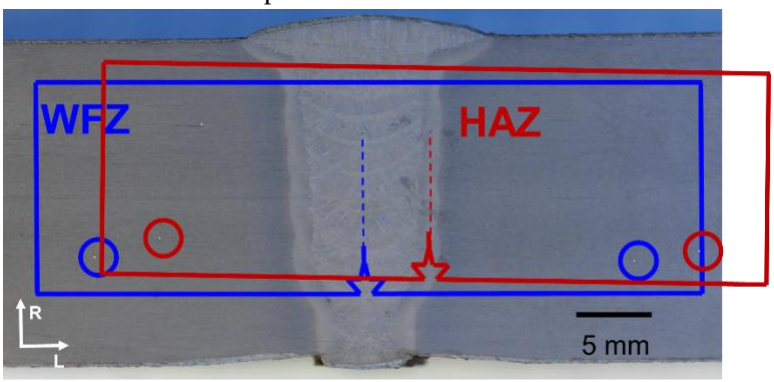

Figure 3 – Approximate location of ESE(T) specimens for measurement of fatigue crack growth rates of WFZ and HAZ. The dashed line represents the crack extension from the machined notch. The HAZ specimen was slightly tilted, compared to the WFZ specimen, to ensure the crack extension remained in the HAZ throughout the fatigue test.

2.2 FCGR Measurements

Fatigue crack growth rate testing was performed in high purity (99.9999%) hydrogen at room temperature, 293 K, on a servo-hydraulic load frame fitted with a custom-built pressure vessel. The system is designed with dynamic spring energized Teflon® U-cup seals that permit in-situ mechanical loading in high pressure hydrogen gas. More details of the in-situ test setup and operating procedures can be found in previous work [7]. Prior to initializing the test, the pressure vessel was evacuated for a minimum of 20 minutes followed by purging with high purity helium to 14 MPa four times. The system was then purged four successive times with high purity hydrogen, before filling to the test pressure of 21 MPa hydrogen. Triplicate tests were performed of each location of the pipe: base metal (BM), weld fusion zone (WFZ), and heat affected zone (HAZ). Tests were performed at a frequency of 1 Hz and at a loading ratio of R = 0.5. The test pressure selected (21 MPa) was identified as an upper bound for hydrogen pipelines based on the recommendations of the ASME B31.12 Hydrogen Piping and Pipeline Code committee. The test frequency of 1 Hz was selected as a compromise of testing efficiency and determining the upper bound FCGR. In general, hydrogen accelerated fatigue crack growth (HA-FCG) rates tend to increase as testing frequency decreases, however, testing at very low frequencies often requires inefficient test durations. Previous work performed on an X52 pipeline steel [8] measured an increase by a factor of only two when test frequency was decreased from 1 to 0.1 Hz, additionally similar FCGRs were measured for test frequencies from 0.001 to 0.1 Hz.

Fatigue crack growth rate curves (da/dN versus ΔK) were measured using either constant load amplitude or K-control conditions. Both methods produced consistent fatigue crack growth rate (FCGR) curves. A load cell is located inside the pressure vessel to ensure precise measurement of the load on the specimen. For measurement of displacement, a front face linear variable differential transformer (LVDT) was used on the C(T) specimens and a clip gauge was used on the ESE(T) specimens. Crack size was determined by unloading compliance. Optical measurements of the initial and final crack lengths were used as fixed bounds to correct crack lengths measured by unloading compliance, and these corrected crack lengths were used with applied loads to determine stress intensity factors. The seven-point

polynomial method [9] was used to calculate the FCGR as a function of applied stress intensity factor range (ΔK). These methods are consistent with ASTM E647 [9].

2.3 Residual Stress Measurements

Residual stress measurements using the slitting method [10-12] were performed on BM, WFZ, and HAZ specimens that were identical to the specimens used for fatigue testing, except that precracks were not present on residual stress specimens. Slitting was performed on the fracture plane of each specimen (i.e., along the dotted line in Fig. 3) to measure residual stress acting to open the crack as a function of position across the specimen width, $\sigma_{res}(x)$, and to determine the residual stress intensity factor as a function of crack length, $K_{res}(a)$. Each specimen was prepared with a metallic foil strain gauge bonded to the specimen back face (the upper edge of the specimen in Fig. 3) where it intersects the fracture plane. A wire electrical discharge machine (EDM) was used to extend a slit along the fracture plane, in increments of slit depth, a, while recording the relaxation of residual stress at the strain gauge. To protect the strain gauge from dielectric cutting fluid, the gauge was waterproofed with silicone. To improve precision, a second strain gauge was mounted to identical material and used for bridge-based temperature compensation. Strain versus slit depth data, ε(a), were then used to determine σ_{res} (x) and $K_{res}(a)$.

Residual stress σ(x) was determined from ε(a) using the pulse-regularization technique [12] which assumes the residual stress distribution can be represented by a sum of basis functions each multiplied by an unknown coefficient. Assuming elastic deformation allows the unknown coefficients to be expressed as a linear system, with a compliance matrix relating the unknown coefficients to measured strain at the set of cut depths. The compliance matrix is specific to the specimen geometry, strain gage details (size and location), and cut depths, can be computed using a finite element simulation [11, 12]. In the pulse-regularization technique, the basis functions are piecewise constant stress (unit pulses) and the coefficients therefore correspond to residual stress over each cut-depth increment. Regularization is used to provide a smooth residual stress distribution that is robust to noise in the strain data. The regularization parameter is adjusted during data analysis such that the misfit of the regularized strain signal indicates a uniform noise signal.

The residual stress intensity factor $K_{res}(a)$ was determined from ε(a) using the methods described earlier by Schindler, *et al.* [13] using

$$K_{res}(a) = \frac{E'}{Z(a)} \frac{d\varepsilon(a)}{da} \tag{1}$$

where E' is the generalized elastic modulus, Z(a) is a geometry dependent influence function, and a is crack length. For a rectangular specimen, like the ESE(T), Z(a) can be obtained using the algebraic expression provided by Schindler and Bertschinger [14]. Elastic modulus was assumed to be Young's modulus of 207 GPa (i.e., plane stress was assumed, since the specimens are thin). The derivative in Eq. 1 was computed by fitting strain data to a moving 5-point quadratic polynomial and evaluating the derivative analytically.

2.4 Correlation and Correction of FCGR Data

Experimental tests are conducted at a fixed cyclic load ratio, defined as the minimum cyclic load, P_{min}, divided by the maximum cyclic load, P_{max}; however, residual stresses impact the calculated stress

ratio as a function of crack length. Here we differentiate between the applied load ratio, R_{app}, which depends on applied load only

$$R_{app} = K_{min\text{-}app}/ K_{max\text{-}app}= P_{min} / P_{max} \quad (2)$$

and the total stress ratio $R_{tot}(a)$ that includes $K_{res}(a)$

$$R_{tot}(a) = (K_{min\text{-}app}(a) + K_{res}(a))/ (K_{max\text{-}app}(a) + K_{res}(a)) \quad (3)$$

where $K_{min\text{-}app}(a)$ and $K_{max\text{-}app}(a)$ are cyclic stress intensity factors at minimum and maximum applied load. It is significant that R_{app} is independent of crack length while $R_{tot}(a)$ is crack-length dependent. Typical tests of materials free of residual stress produce FCGR as a function of ΔK at fixed stress ratio (e.g. $R_{app} = R_{tot}$); however, FCGR tests of materials that contain residual stress are performed at fixed R_{app} but varying $R_{tot}(a)$. Note that the stress intensity factor range, ΔK, is independent of non-zero $K_{res}(a)$ because $K_{res}(a)$ appears in both minimum and maximum stress intensity factors, cancelling when they are subtracted to obtain ΔK (i.e., $\Delta K = \Delta K_{app}$). Therefore, when testing residual stress bearing material, there is a need to correct FCGR data so they can be used in structural assessments that take FCGR input as functions of ΔK and R.

In order to assess FCGR data from the tests on welded specimens, we employ the analysis methodology outlined by Donald and Lados [15] and further detailed by James, *et al.* [16] to transform the FCGR data to a single value of stress ratio, $\bar{R}$, so that the data are useful for design. A first step in the analysis is to collapse the FCGR data for the effect of maximum stress intensity factor using a normalized stress intensity factor, $K_{norm}(a)$ [15]:

$$K_{norm}(a) = (\Delta K(a))^{1-n} * (K_{max-app}(a) + K_{res}(a))^n \quad (4)$$

where n is a parameter for K_{max} sensitivity (n = 1 makes K_{norm} depend only on K_{max}, while n = 0 makes K_{norm} depend only on ΔK). To determine n, three FCGR tests were performed on X100 base metal in air at R = 0.1, R=0.5, and R=0.7, where the base metal specimens were free of residual stress. Crack closure was not observed in any of the tests, likely due to the higher load ratios, therefore, no crack closure adjustments were made. A value of n was determined by adjusting n while observing the FCGR versus K_{norm} test data gathered at different load ratios. Figure 4a shows the FCGR data versus ΔK and Fig. 4b shows FCGR data versus K_{norm} for n = 0.25, which was selected by a visual best fit. Testing in hydrogen gas was only performed at R=0.5, therefore the n values were not determined for each microstructural region and in each environment. The n value determined is consistent with values for other structural metals reported in the literature [15, 16], and was assumed valid for WFZ, HAZ, and BM specimens. Data from [17] were compared for an X60 steel tested in air and 5.5 MPa H_2 gas at R=0.1 and R=0.5, and it was found that a similar n value of 0.15 was sufficient to collapse both K_{norm} curves for air and hydrogen. This suggests that the n value determined in air is also applicable in hydrogen. By using Eq. 4 with n = 0.25, a K_{norm} master curve was determined for data from the tests in WFZ, HAZ, and BM specimens. The K_{norm} curve was then transformed using the Walker equation [16] so it reflected the FCGR at a specific stress ratio $\bar{R}$:

$$\Delta K_{corr} = K_{norm} * (1 - \bar{R})^n \quad (5)$$

where n = 0.25, $\bar{R}$ is taken as 0.5, and the subscript corr indicates the correction to account for the effect of varying $R_{tot}(a)$ on FCGR.

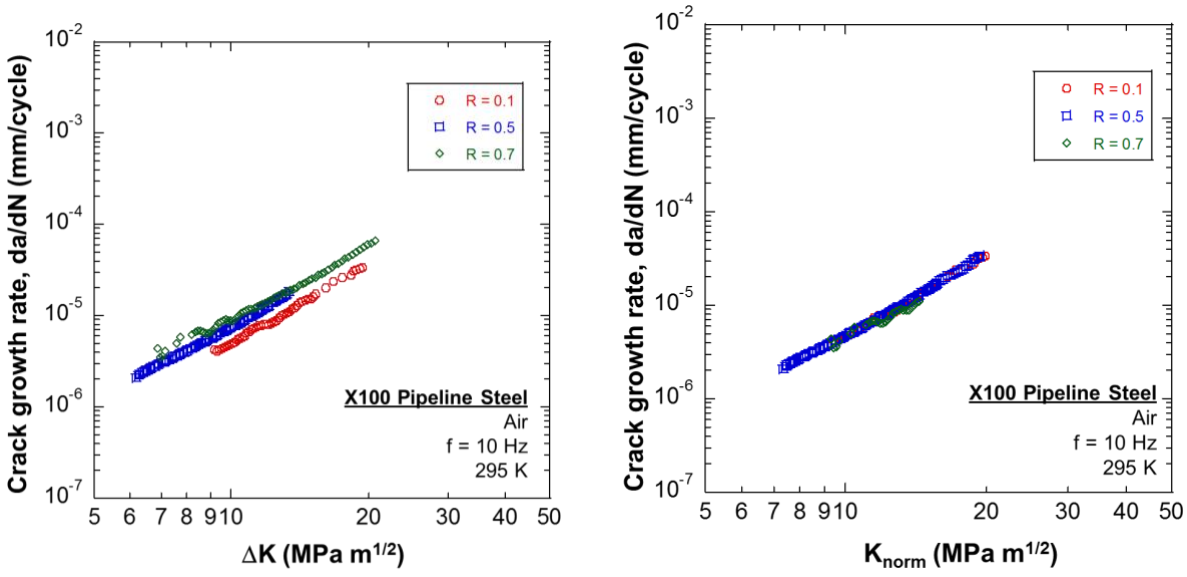

(a) (b)

Figure 4 – (a) FCGR curves for X100 base metal performed in air at 10 Hz, (b) Fatigue crack growth rate data versus K_{norm} for data from (a) according to Eq. 4 using n = 0.25.

3. Results and Discussion

3.1 FCGR Measurements

The effects of hydrogen accelerated fatigue crack growth (HA-FCG) are apparent in Fig. 5 by the observable increase in FCGR for the specimens tested in hydrogen relative to FCGR found in tests performed in air. For example, at ΔK values greater than 12 MPa $m^{1/2}$, the crack growth rate of the base metal is more than 30 times greater in hydrogen than in air. At lower ΔK values, the FCGRs appear to converge with the data in air, specifically for the HAZ tests. Repeatability was observed among the triplicate tests for the BM and HAZ. The WFZ curves exhibited some variability by means of inflections in the curves, however, further analysis suggested that the inflections were caused by crack propagation through the multiple weld passes, as shown in Fig. 3. One possible cause of this variability is the periodicity of residual stresses with each weld pass which will be discussed in further detail below. A comparison of the three regions tested in hydrogen shows that the FCGRs in the WFZ were slightly greater than those in the BM, which were greater than those in the HAZ. It is important to note that the FCGR data in Fig. 5 are reported versus ΔK, but are not at a constant $R_{tot}(a)$ due to the effects of residual stress. It will be shown that accounting for $K_{res}(a)$ produces a measurable effect on $R_{tot}(a)$, so the data shift when transformed and plotted versus ΔK_{corr}.

Following the fatigue tests, the specimens were fractured open and examined. Figure 6 shows optical images of the fracture surfaces for the BM, HAZ, and WFZ tested in hydrogen along with the BM tested in air. Three distinct regions can be observed on all fracture surfaces of the fatigue specimens: fatigue pre-crack in air, fatigue in air or H_2, and final overload fracture in air. On the weld fracture surfaces (Fig. 6d), periodic features are observed which were determined to be associated with each weld pass. The distance between the rough fracture surface features shown in Fig. 6d are consistent with the weld pass spacing shown in Fig. 1b, e.g. between 2 and 2.5 mm. It was also observed that the distance between the inflections in the weld FCGR curves in Fig. 5 were consistent with the physical distance

between weld passes. Therefore, the presence of multiple weld passes appears to influence the fatigue crack growth rate.

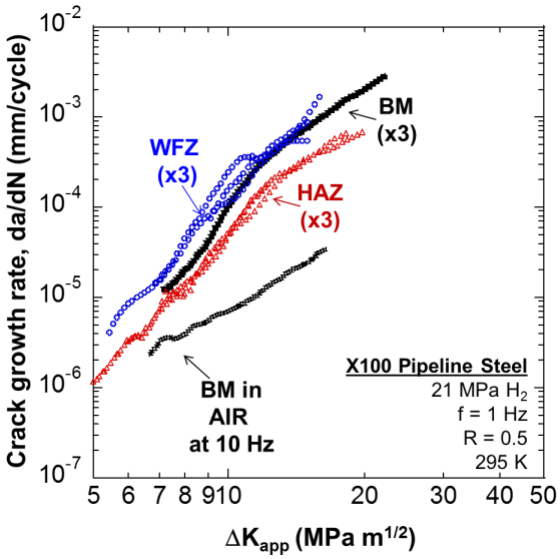

Figure 5 – Fatigue crack growth rate (da/dN versus ΔK_{app}) curves of X100 welded pipeline steel tested in 21 MPa hydrogen gas at R_{app} = 0.5 and frequency of 1 Hz. BM = base metal, WFZ = weld fusion zone, HAZ = heat affected zone. BM tests in air were performed at 10 Hz.

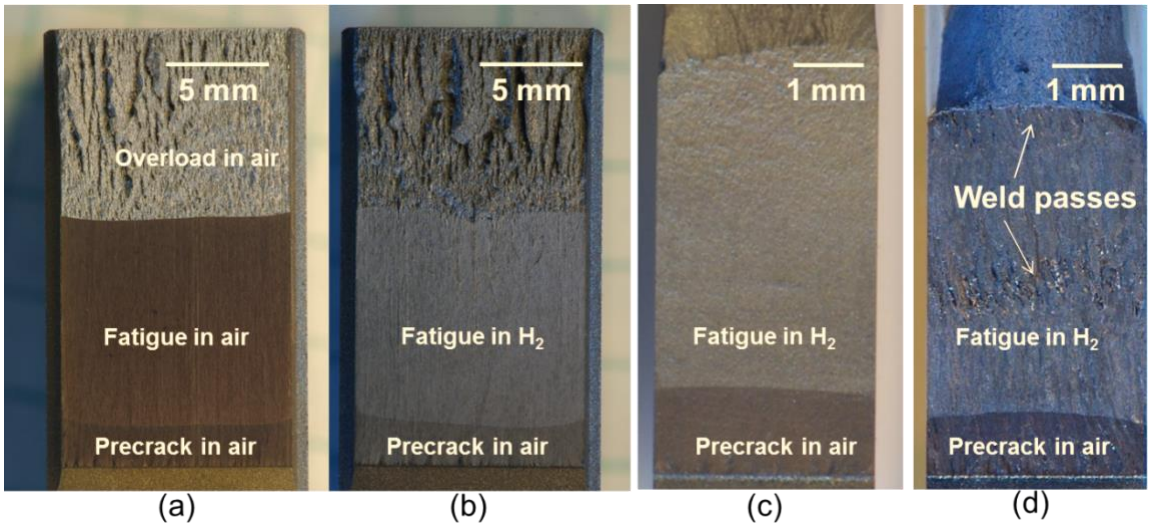

Figure 6 – Fracture surfaces of select fatigue specimens: (a) BM tested in air, (b) BM tested in H_2, (c) HAZ tested in H_2, (d) WFZ tested in H_2.

3.2 Residual Stress Measurements

Residual stress as a function of position along the fracture plane is shown in Fig. 7 for specimens taken from the BM, WFZ, and HAZ. Stress in the BM specimen (e.g. BM-9) was negligible throughout the entire width, whereas the WFZ specimens (e.g. W6 and W7) and HAZ specimens (e.g. H4 and H5) exhibited significant residual stresses. It should be noted that the residual stress measurements were taken on CT specimens for the BM and ESE specimens for the WFZ and HAZ, thus the distance from the front

face varies in Fig. 7 for these two different specimen geometries. The stress measurements were repeatable for duplicate measurements in the WFZ and HAZ specimens. In the WFZ, the residual stresses ranged from over +200 MPa to -300 MPa, a significant magnitude of residual stress. In the HAZ specimens, stresses are tensile at short crack lengths (e.g. near the I.D. of the pipe and the weld root), compressive near the mid-thickness, and near zero towards the O.D. of the pipe and the weld crown. Stress in the WFZ specimens are similar to the HAZ specimens, but with the addition of high-magnitude, short range tension-compression variations that are on the scale of the weld passes.

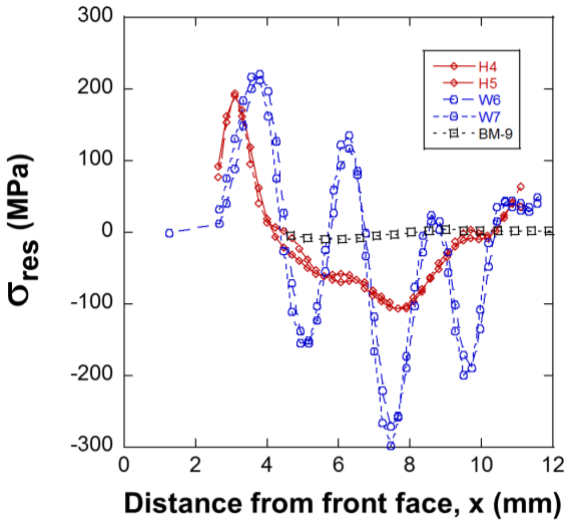

Figure 7 – Residual stress as a function of distance from front face across the specimen width for BM (BM-9), WFZ (W6, W7), and HAZ (H4, H5) specimens.

The measured values of K_{res} as a function of crack size are shown in Fig. 8. The values of K_{res} are negligible for the base metal specimen but significant for the WFZ and HAZ specimens. In the HAZ, K_{res} is consistently positive and diminishes to negligible values at large crack size. In the WFZ, K_{res} is also consistently positive and has periodic variation with crack size. The variations of K_{res} with crack size (Fig. 8) are consistent with the variations of residual stress with position (Fig. 7), since K_{res} is a weighted integral of residual stress [Ref: Wu X, Carlsson J. Weight functions and stress intensity factor solutions. Oxford: Pergamon Press; 1991]: the slope of K_{res} is positive where stress is positive and the slope is negative where stress is negative. The K_{res} values as a function of crack size are compared to an etched image of the weld showing multiple weld passes in Fig. 9. The periodicity of the K_{res} peaks appears to be in phase with the periodicity in weld passes, which is on the order of 2 to 2.5 mm. This is also consistent with the periodicity observed in the inflections of the FCGR curves for the WFZ in Fig. 5. Overall the residual stress intensity factors are significant and positive for the WFZ and HAZ specimens and are consistent in duplicate tests.

Residual stress affects the stress ratio, with positive $K_{res}(a)$ elevating the stress ratios above the applied $R_{app} = 0.5$. The total stress ratio, $R_{tot}(a)$ calculated according to Eq. 3, is shown in Fig. 10. Because the $K_{res}(a)$ is negligible for the BM specimen, the $R_{tot}(a)$ is very close to 0.5, while for the WFZ and HAZ specimens $R_{tot}(a)$ is elevated above 0.5 at shorter crack lengths, but similar to 0.5 at longer crack lengths.

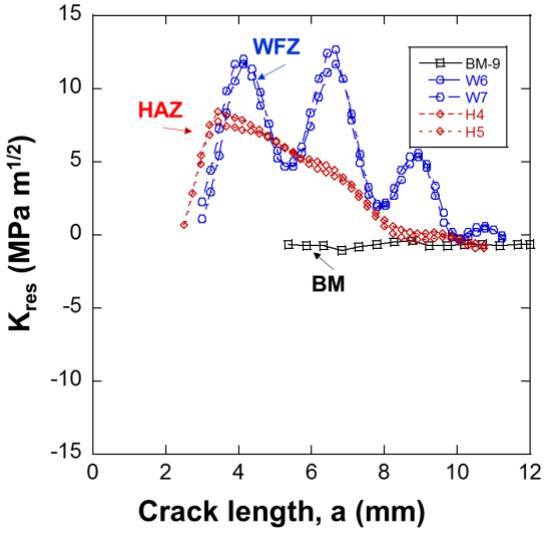

Figure 8 – Residual stress intensity factor (K_{res}) versus crack length for BM, WFZ, and HAZ specimens. Duplicates were performed on WFZ (W6, W7) and HAZ (H4, H5) specimens.

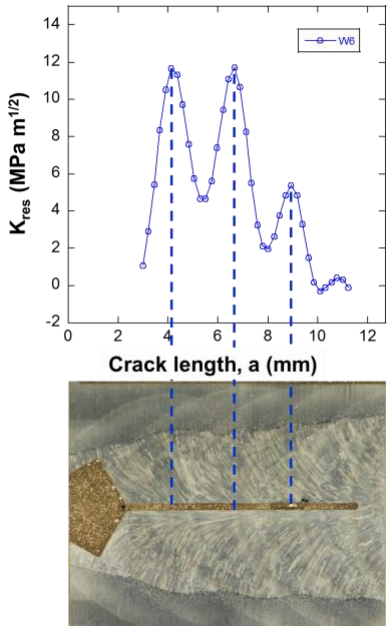

Figure 9 – K_{res} versus crack length for the weld (W6) showing periodicity of the peaks in K_{res} with the weld passes.

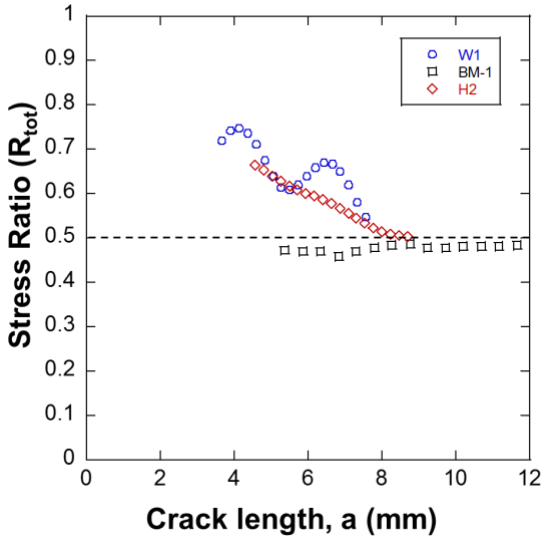

Figure 10 – Total stress ratio (R_{tot}) versus crack length for the weld fusion zone (W1), base metal (BM-1), and heat affected zone (H2).

3.3 Correlation and Correction of FCGR Data

Due to the repeatability of the triplicate FCGR tests, a single curve was corrected according to the methodology described above using Eq. 5 for each region of the X100 pipeline steel weld (BM, WFZ, HAZ) and then plotted in Fig. 11 for a specified stress ratio of $\bar{R} = 0.5$. The residual stress-free data are plotted as da/dN versus ΔK_{corr}. The effects of residual stress on the fatigue crack growth rates can be observed by comparing the residual stress corrected data in Fig. 11 to the non-corrected data in Fig. 5. Negligible residual stresses were measured in the BM data so the BM curves are nearly identical in both Fig. 5 and Fig. 11 and can be used as a reference. Once residual stress effects were removed and the FCGR were plotted at the specified $\bar{R} = 0.5$, a significant shift in the curve to the right was observed for the WFZ and HAZ data compared to the negligible change in the base metal data. In other words, when residual stress effects were removed, the da/dN curve shifted to higher ΔK_{corr} resulting in lower crack growth rates for a given ΔK. The WFZ and HAZ exhibited a similar shift to the right, although with the HAZ shift being lesser in magnitude. For a given ΔK, the FCGR of the WFZ was greater in Fig. 5 than Fig. 11 because of the higher total stress ratio in Fig. 5. The expected trend is an elevation of FCGR at higher stress ratio for a given ΔK, because K_{max} is higher. For example, at a ΔK = 10 MPa $m^{1/2}$ for R = 0.5, 0.6, and 0.7, the K_{max} is 20, 25, and 33 MPa $m^{1/2}$, respectively. It is therefore not surprising that, in the WFZ specimens, FCGR is elevated relative to FCGR in BM specimens when the data are not corrected for the effect of residual stress, as in Fig 5, because the tests were essentially performed at R-ratios closer to 0.6 and 0.7. The HAZ specimens also had elevated R-ratios close to 0.6, which when corrected shifted the curve to the right.

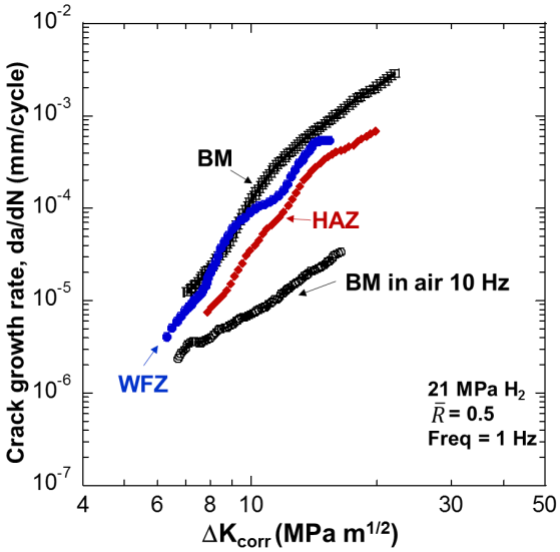

Figure 11 – Residual stress-free FCGR curves (da/dN versus ΔK_{corr}) for X100 base metal (BM), weld fusion zone (WFZ), and heat affected zone (HAZ).

It is noteworthy that once FCGR data are corrected for the influence of residual stress, as in Fig. 11, the FCGR data from BM and WFZ specimens are similar over the range of ΔK_{corr} and the FCGR data from HAZ specimens exhibit lower crack growth rates. The transformed FCGR data, in Fig. 11, show that FCGR in BM specimens provide an upper bound for data from the three regions tested after the effects of residual stress are removed. This observation is significant as it highlights the importance of accounting for residual stress effects to enable useful comparisons among the different regions of the welded pipe. One complicating factor of fatigue crack growth data in welds is that the influence of residual stress is often ignored and the magnitudes of residual stresses in test specimens are unknown. The methodology used in this study to partition the effects of residual stress from the fatigue crack growth rate tests improve their fidelity, which will improve safety.

4. Conclusions

Fatigue crack growth rate (FCGR) tests were performed on specimens removed from X100 girth welded steel pipe. Tests were carried out at 10 Hz in air for specimens removed from the base metal and at 1 Hz in high pressure (21 MPa) hydrogen gas for specimens removed from the weld fusion zone (WFZ), heat affected zone (HAZ), and base metal (BM). All tests were performed at an applied load ratio of 0.5. Measurements were made on replicate specimens using the slitting method to determine residual stress and the residual stress intensity factor. Significant residual stresses were found in WFZ and HAZ specimens and negligible residual stresses were found in BM specimens. A methodology was used to remove the effects of residual stress from the FCGR data by normalizing the data with respect to maximum stress intensity factor, and then re-introducing stress ratio effects to facilitate the formation of FCGR data independent of residual stress effects. Removal of residual stress effects resulted in shifts of the FCGR data such that FCGR in X100 base metal provided an upper bound compared to rates in the WFZ and HAZ. This observation is significant, and only becomes apparent upon removing residual stress effects from FCGR data for the different regions of weld.

Acknowledgements:

The authors would like to thank B. Davis, J. Benton, J. Campbell, A. Gardea, R. Nishimoto, and G. Evans for their assistance in executing tests, metallography, microscopy, and discussions. Additionally, the authors are appreciative for fruitful discussions with A. Slifka, E. Drexler, R. Amaro, and C. San Marchi. This work was funded by the Fuel Cell Technology Office. Sandia National Laboratories is a multimission laboratory managed and operated by National Technology and Engineering Solutions of Sandia, LLC., a wholly owned subsidiary of Honeywell International, Inc., for the U.S. Department of Energy's National Nuclear Security Administration under contract DE-NA-0003525.

References

[1] Hydrogen Pipeline Working Group Workshop, U.S. Department of Energy, Augusta, GA, 2005, www1.eere.energy.gov/hydrogenandfuelcells/wkshp_pipeline_group_2005.html.

[2] Ronevich JA, Somerday BP. Assessing gaseous hydrogen assisted fatigue crack growth susceptibility of pipeline steel weld fusion zones and heat affected zones. Mater Perf and Char 2016;5(3):290-304.

[3] Ronevich JA, Somerday BP, San Marchi CW. Effects of microstructure banding on hydrogen assisted fatigue crack growth in X65 pipeline steels. Int J Fatigue 2016;82(3): 497-504.

[4] Slifka AJ, Drexler ES, Nanninga NE, Levy YS, McColskey JD, Amaro RL, Stevenson AE. Fatigue crack growth of two pipeline steels in a pressurized hydrogen environment. Corr Sci 2014;78:313-21.

[5] Ronevich JA, Somerdary BP, Feng Z. Hydrogen accelerated fatigeu crack growth of friction stir welded X52 pipe. Int J Hydrogen Energy 2017;42(7):4259-68.

[6] Fekete JR, Sowards JW, Amaro RL. Economic impact of applying high strength steels in hydrogen gas pipelines. Int J Hydrogen Energy 2015;40:10547-58.

[7] Somerday BP, Campbell JA, Lee KL, Ronevich JA, San Marchi C. Enhancing safety of hydrogen containment components through materials testing under in-service conditions. Int J Hydrogen Energy 2017;42(11):7314-21.

[8] Somerday BP, Sofronis P, Nibur KA, San Marchi C, Kirchheim R. Elucidating the variables affecting accelerated fatigue crack growth of steels in hydrogen gas with low oxygen concentrations. Acta Mater 2013;61:6153-70.

[9] ASTM E647-11 Standard Test Method for Measurement of Fatigue Crack Growth Rates. West Conshohocken, PA, 2011.

[10] Prime MB. Residual stress measurement by successive extension of a slot: The crack compliance method. App Mech Reviews 1999;52(2):75-96.

[11] Hill MR. The Slitting Method in Practical Residual Stress Measurement Methods. West Sussex, UK: John Wiley & Sons; 2013:89-108

[12] Schajer GS, Prime MB. Use of Inverse Solutions for Residual Stress Measurements. J Eng Mater Tech 2006;128:375-82.

[13] Schindler HJ, Cheng W, Finnie I. Experimental Determination of Stress Intensity Factors due to Residual Stresses. Exp Mech 1997;37(3):272-79.

[14] Schindler HJ, Bertschinger P. Some Steps Towards Automation of the Crack Compliance Method to Measure Residual Stress Distributions. Proceedings of the Fifth Int. Conference on Residual Stresses 1997:682-87.

[15] Donald JK, Lados DA. An intergrated methodology for separating closure and residual stress effects from fatigue crack growth rate data. Fatig Fract Eng Mater Struct 2006;30:223-30.

[16] James M, Maciejewski K, Wang G, Ball D, Bucci R. A Methodology for Partitioning Residual Stress Effects from Fatigue Crack Growth Rate Test Data. Mater Perf Char 2016;5(3):194-214.
[17] San Marchi C, Somerday B, Nibur K, Stalheim D, Boggess T, Jansto S. Fracture and Fatigue of Commerical Grade API Pipeline Steels In Gaseous Hydrogen. Proceedings of ASME PVP 2010:1-8.